Hindawi Publishing Corporation
Journal of Nanomaterials
Volume 2014, Article ID 986809, 7 pages
http://dx.doi.org/10.1155/2014/986809

Research Article

Photocatalytic Property of $Fe_3O_4/SiO_2/TiO_2$ Core-Shell Nanoparticle with Different Functional Layer Thicknesses

Junyang Li,[1,2] Libo Gao,[1,2] Qiang Zhang,[1,2] Ruiting Feng,[1,2] Hongyan Xu,[1,2] Jie Wang,[3] Dong Sun,[1,2,4] and Chenyang Xue[1,2]

[1] *Key Laboratory of Instrumentation Science and Dynamic Measurement of Ministry of Education, North University of China, Taiyuan, Shanxi 030051, China*
[2] *Science and Technology on Electronic Test & Meaurement Laboratory, North University of China, Taiyuan, Shanxi 030051, China*
[3] *College of Environmental Science and Engineering, Taiyuan University of Technology, Taiyuan, Shanxi 030051, China*
[4] *Department of Mechanical and Biomedical Engineering, City University of Hong Kong, Kowloon, Hong Kong*

Correspondence should be addressed to Dong Sun; medsun@cityu.edu.hk and Chenyang Xue; xuechenyang@nuc.edu.cn

Received 19 November 2013; Revised 20 January 2014; Accepted 20 January 2014; Published 24 February 2014

Academic Editor: Christian Falconi

This study examined the different properties of $Fe_3O_4/SiO_2/TiO_2$ (FST) core-shell nanoparticles encapsulated for one to five different times, represented as FST1 to FST5, respectively. These FST nanoparticles were obtained using the carbon reduction and sol-gel methods, and their properties were characterized by various tools, such as scanning electron microscopy, transmission electron microscopy, X-ray diffraction, vibratory sample magnetometer, laser granularity apparatus, and specific surface area analyzer. The relationship between irradiation time and decoloration ratio indicates that FST2 demonstrated significant efficiency in the decolorization of methyl orange (MO) under UV light. Further study on recycle activity showed that FST2 had a high decoloration rate after four cycles of photocatalysis, and its degradation of MO was well aligned with the apparent first-order kinetic equation. Furthermore, FST2 exhibited the highest apparent rate in the first cycle. All these results demonstrate that the recoverable FST2 possessed excellent photocatalytic activity while maintaining outstanding stability for further applications, such as managing environmental pollution.

1. Introduction

Nanoparticles have been widely used in numerous industrial processes [1–4]. One of these applications is the treatment of chemicals and biological molecules in wastewater. As high as 15% of azo dyes are lost annually during the production of textile, paper, leather, ceramic, cosmetics, ink, and food [5]. Given its high free hydroxy production, TiO_2 nanoparticles have been used in photocatalytic oxidation degradation [6–11] to obtain an effective optical spectrum, high chemical and biological inertness, nontoxicity, and low cost. Relevant studies have received considerable attention in recent years [11–15].

Numerous studies on the photocatalytic effect of core-shell structures based on titanium dioxide, silica layer, and magnetic core have been reported in the literature [16–22]. A study [16] showed that core-shell structure $TiO_2/BaFe_{12}O_{19}$ composite nanoparticles can effectively photodegrade organic pollutants in the dispersion system. As reported in [17], the SiO_2/TiO_2 particles exhibit higher photocatalytic activity than pure TiO_2. To optimize photocatalytic performance, several studies [18–20] synthesized $Fe_3O_4/SiO_2/TiO_2$ (FST) particles for the decomposition of acid [19, 20] or methyl orange (MO) dye [21], which can be recycled easily using a magnetic field method because of the existence of Fe_3O_4. The amount of TiO_2 is closely related to the functional layer and serves a key function in the photocatalytic system. The studies [22, 23] analyzed the SiO_2/TiO_2 composite nanoparticles for multistep shell coating of TiO_2 and found that the number of coating steps is not more than three. A study [19] reported that FST particles maintain high degradation rate and catalyst recovery even

after being used for eight times. All these results indicated that the properties of FST core-shell nanoparticles can be optimized through TiO_2 coating and recovery for a suitable number of times, without introducing any additional doping materials that may result in secondary pollution.

This paper presents our research on the properties of FST core-shell nanoparticles by coating TiO_2 functional layers at different times. The coating activity aimed to enhance the photocatalytic capacity of the functional nanoparticles. To characterize the properties of FST nanoparticles, transmission electron microscopy (TEM) was used to test the morphology, and X-ray diffraction (XRD) was used to verify the components of these particles. Through vibratory sample magnetometer (VSM) and Brunauer-Emmett-Teller (BET) analysis, the magnetic property and specific surface area of these FST particles were successfully observed. The recycle experiment was performed to demonstrate the recyclability of the FST particles. The experimental results illustrate that the degradation of MO was in agreement with the apparent first-order kinetic equation, thereby verifying the photocatalytic capability and stability of the FST particles.

2. Methodology

2.1. Reagents and Apparatus. Ferric chloride, tetraethoxysilane (TEOS), tetrabutyl orthotitanate (TBOT), alcohol, hydrochloric acid, and nitric acid were all provided by Sinopharm Chemical Reagent Co., Ltd. (Shanghai, China). Titanium dioxide (TiO_2) powder sample, used as a contrast photocatalyst in our study, was commercial Degussa P25 with 80% anatase and 20% rutile produced by the Degussa AG Company in Germany. MO (λ_{max} = 462.5 nm) obtained from Sigma was used as a model pollutant. Deionized water with 18.25 MΩ was purified using an ultrapure system. With a JEOL JEM-1200EX TEM, measurements were performed with an accelerating voltage of 200 kV. The surface morphology of the composite nanomaterials was observed using a S4700 scanning electron microscope (SEM). XRD measurements were also performed by a Bruker D8 Advance XRD system. Magnetic properties were characterized by a Lake shore 7307 VSM. The average size of particles was tested by a Mastersize 2000 Laser Granularity Apparatus. The specific surface area was measured using a QUADRASORB SI specific surface area instrument. The absorbance of the degraded solution was tested by a 721G visible spectrophotometer.

2.2. Synthesis of Core-Shell Structure FST Magnetic Particles. The Fe_3O_4 magnetic particles were obtained using the carbon reduction method [13] and modified with SiO_2. The Fe_3O_4 particles were placed in a beaker with 100 mL of alcohol, to which 15 mL of TEOS was added after the temperature reached 50°C. Thereafter, 0.97 mL of hydrochloric acid and a small amount of deionized water were added into the collosol. After 3 h, the residual collosol was poured out, and the particles at the bottom of the beaker were attracted by a magnet. The wet particles were placed in a quartz Petri dish and heated at 500°C for 2 h under −0.2 Trom vacuum conditions. After milling, Fe_3O_4/SiO_2 particles were finally obtained.

The Fe_3O_4/SiO_2 particles were then encapsulated with different TiO_2 shell thicknesses. First, the particles were placed in a beaker with TBOT and alcohol. The beaker with the collosol and particles was treated under ultrasound for 10 min and stirred for 20 min. Second, deionized water was slowly added with continuous stirring. The ratios of ester and alcohol over water were 30.3 : 1 and 12.5 : 1, respectively. Third, the particles were heated at 500°C for 2 h under −0.2 Trom vacuum conditions. After milling, FST1 was obtained. The other types of nanoparticles (e.g., FST2, FST3, FST4, and FST5) with different TiO_2 shell thicknesses were also obtained by following the same procedures.

3. Results and Discussion

3.1. Characterization of FST Particles. The morphologies of SiO_2/TiO_2 core-shell particles with various coating steps are shown in Figure 1. Figure 1(a) shows that the FST1 particles were successfully encapsulated by a TiO_2 layer even though the thickness of the layer was extremely thin. This result may be caused by particles with low photocatalytic performance. Figure 1(b) shows that the TiO_2 layer of FST2 was thicker and more uniform than that of FST1. The TEM image of the distribution of FST2 particles is shown in Figure 1(c), which shows small clusters of FST particles with good dispersion. The TEM image of FST3 in Figure 1(d) reveals that FST3 also had a uniform coating layer and the amount of TiO_2 in FST4 (Figure 1(e)) was slightly less than that in FST3. The TEM image of FST5 in Figure 1(f) shows that the amount of TiO_2 in FST5 was similar to that in FST4 with a shell thickness of approximately 60 nm. More importantly, the TiO_2 layer of one FST5 particle had no magnetic core, which indicates that the nonmagnetic core particles could be generated as the coating times increased.

The morphology of the as-prepared FST nanoparticles was observed by SEM. Figure 2 illustrates the panoramic morphologies of the as-obtained products, which were mainly uniform nanoparticles, with diameters ranging from 400 nm to 500 nm. Figures 2(a) and 2(b) show that the surfaces of the FST1 and FST2 nanomaterials were rough, which resulted in larger specific surface areas, as specified in Table 1. The FST2 particles in Figure 2(c) displayed a certain level of homogeneity in shape and size. The surfaces of the other three nanoparticles, as shown in Figures 2(d), 2(e), and 2(f), became increasingly smooth as the coating times increased, which resulted in a sharp drop in specific surface area.

The structure and phase purity of synthesized Fe_3O_4, SiO_2/TiO_2, and FST nanoparticles under different coating times were determined based on the XRD patterns, as indicated in Figure 3. The XRD pattern of Fe_3O_4 was in agreement with the JCPDS card number 19-0629 and displayed characteristic peaks [at 2θ: 18.2°(111), 30.4°(220), 35.7°(311), 43.4°(400), 57.4°(511), and 63.0°(440)] of the cubic spinel structure. The coating of the amorphous SiO_2 layer did not affect the structure of Fe_3O_4 because no impurity

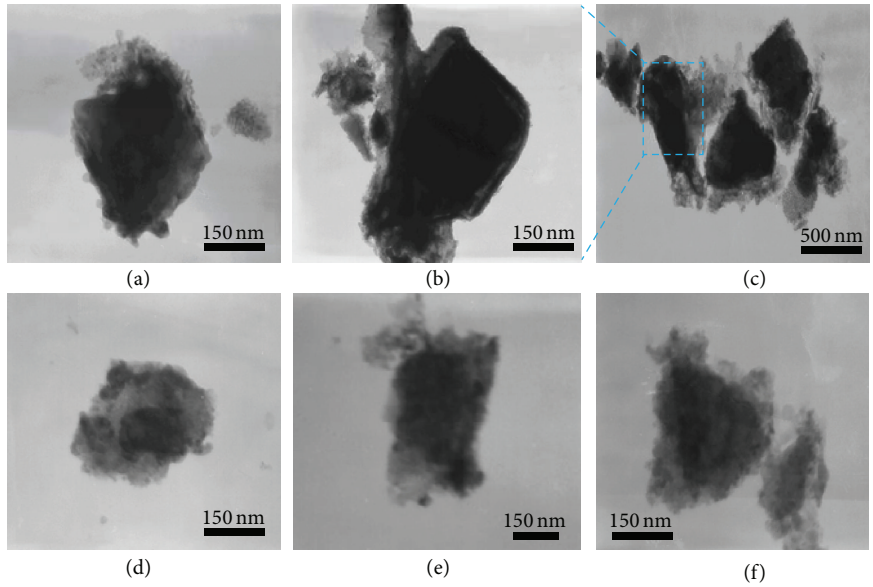

Figure 1: TEM images of (a) FST1, (b) FST2, (c) clusters of FST2 particles, (d) FST3, (e) FST4, and (f) FST5.

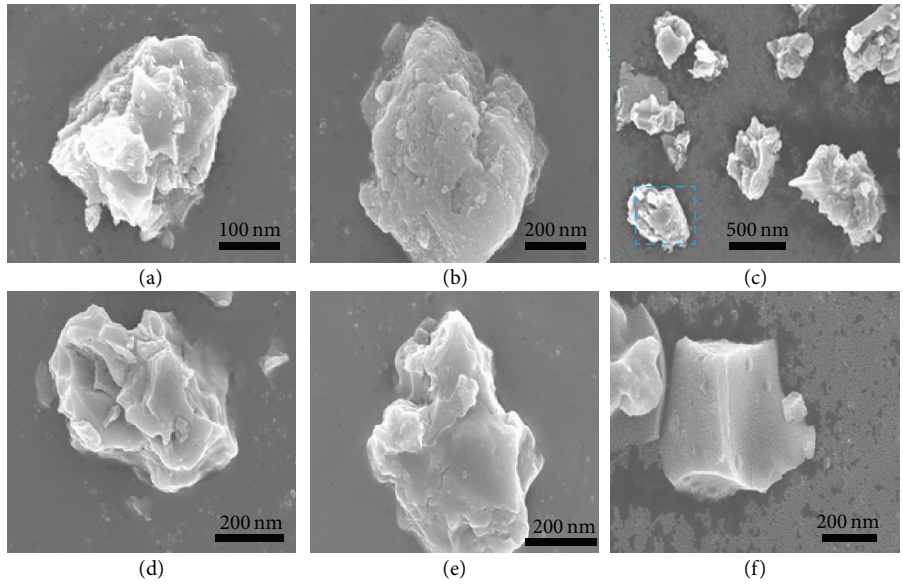

Figure 2: SEM micrographs of (a) FST1, (b) FST2, (c) clusters of FST2 particles, (d) FST3, (e) FST4, and (f) FST5.

was observed. Moreover, FST is composed of anatase TiO_2 (JCPDS card number 21-1272). The peaks at 25.4°(101) and 48.1°(200) reveal the presence of anatase TiO_2 in the synthesized nanocomposites. Notably, the relative intensity of FST2 peaks at 25.4°(101) was larger than that of FST1 but smaller than those of FST3 and FST4, and the peak of FST5 was the largest. We hypothesize that the TiO_2 content can be enhanced as the coating time increases.

Figure 4 and Table 1 show the size distribution spectrum and specific surface areas of the five FST particles and pure TiO_2. The results demonstrate that the average size was 500 nm, as shown in curves (a) and (b) of Figure 4 and the average size of FST2 particles (550 nm) increased by approximately 150 nm compared with that of FST1 (330 nm) as the coating times increased. After titania coating for three

Table 1: Specific surface area of the FST nanoparticles.

Type	BET (m^2/g)
FST1	55.611 ± 2%
FST2	48.392 ± 2%
FST3	7.604 ± 2%
FST4	5.85 ± 2%
FST5	4.58 ± 2%
Pure TiO_2	41.708 ± 2%

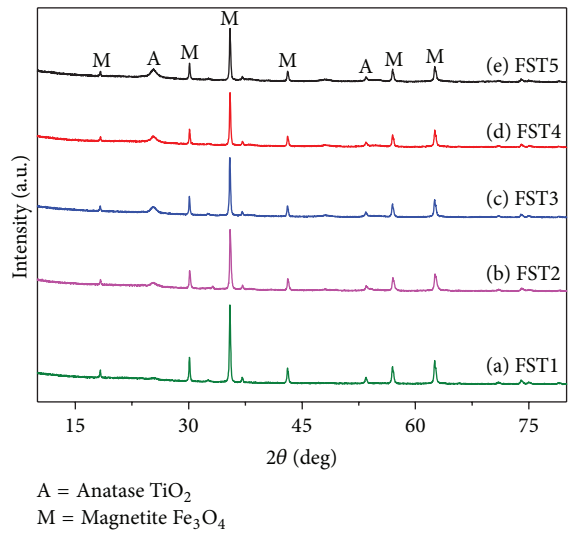

Figure 3: XRD patterns of (a) FST1, (b) FST2, (c) FST3, (d) FST4, and (e) FST5.

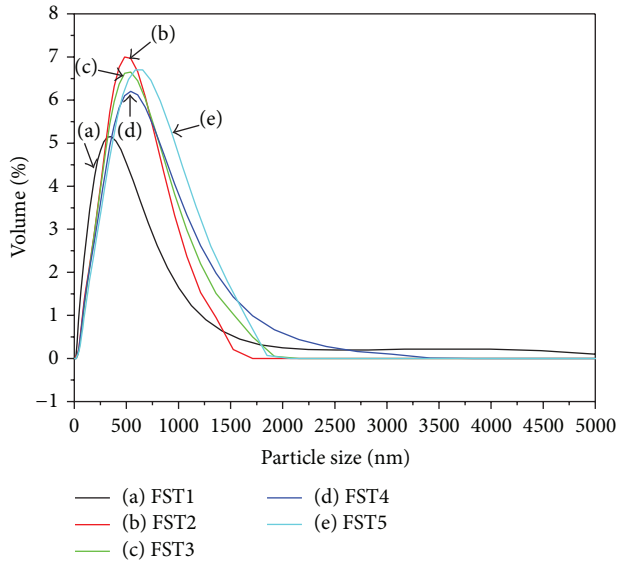

Figure 4: Size distribution spectrum of (a) FST1, (b) FST2, (c) FST3, (d) FST4, and (e) FST5.

times, the size of the FST3 (517 nm) and FST4 (528 nm) particles did not increase as significantly as those of FST2. Instead, as the titania coating steps increased, the specific surface area of FST particles sharply declined (e.g., from FST2 (48 $m^2/g \pm 2\%$) to FST5 (4.58 $m^2/g \pm 2\%$)), as specified in Table 1. This finding indicates that the outermost functional layer became tighter as the titania coating times increased, thereby resulting in a smaller surface area [23]. As shown in the SEM micrographs, the surface of the particles became increasingly smooth because of the reduced photocatalytic degradation capability of FST3, FST4, and FST5 particles.

The magnetization behavior shown in Figure 5 indicates that the saturation intensity of the five FST particles progressively decreased from FST1 (46.5 emu/g) to FST5

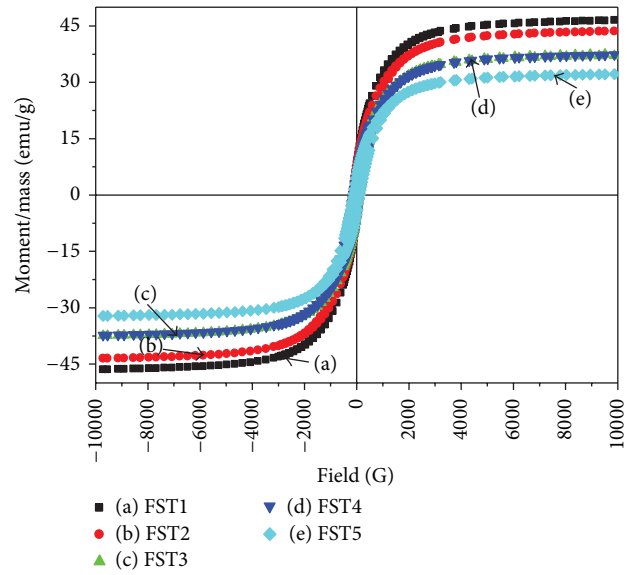

Figure 5: Hysteresis cycles of (a) FST1, (b) FST2, (c) FST3, (d) FST4, and (e) FST5.

(32.2 emu/g). Meanwhile, the remanence of the five types of particles was nearly free so that the particles could not agglomerate. These samples appeared to have a mixture of ferrimagnetic and superparamagnetic properties, with only a minor indication of hysteresis. Although the magnetism of FST5 remained sufficiently high to be magnetically segregated by applying a magnetic field, this property could accelerate the separation of photocatalysts from MO solutions. These recycled materials may be further used in the water treatment process, thereby reducing secondary pollution.

3.2. Photocatalytic Activity. The photocatalytic activity of FST functional particles with different coating times was studied using the decolorization of MO solution as a model pollutant. The experiments were conducted in a 150 mL cylindrical glass reactor equipped with a UV lamp (365 nm, 8 W). The reactor contained 40 mL of MO solution with an initial concentration of 10 mg/L and 0.4 g of FST functional particles. The standard P25 was used as a reference under the same experimental conditions.

Figure 6 shows that the decolorization of MO solution for FST1 reached 25.10%. Previous characterization results showed that the thickness of the TiO_2 functional layer of FST1 was small, which may result in a low degree of decolorization of the MO solution for FST1. Furthermore, the decolorization of MO solution for FST3 during photocatalytic degradation was only 12.25%, whereas those for FST4, FST5, and blank were less than 1%. These results indicate that the photocatalytic degradation of MO solution may be induced by the titania content and specific surface area. Our experimental results reveal that the decoloration of MO solution reached 71% and 85% for P25 and FST2 particles, respectively, after 25 h of UV light irradiation. FST2 exhibited the highest photocatalytic efficiency among the five FST nanoparticles. Meanwhile, the photocatalytic activity of

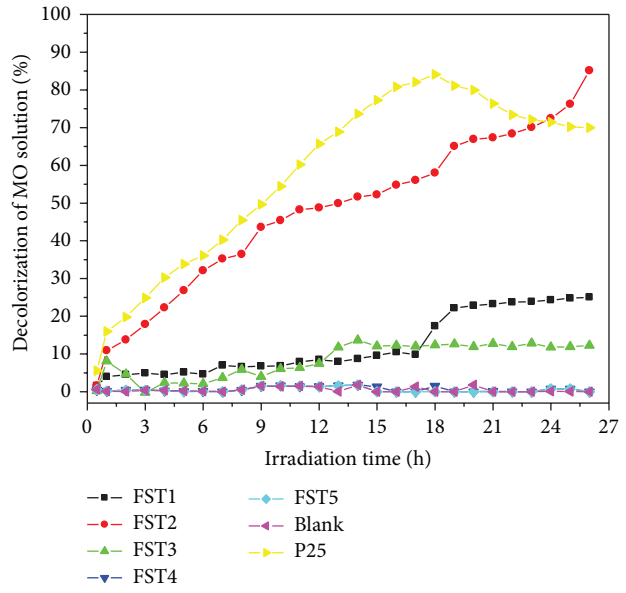

Figure 6: Curves of photocatalytic decoloration of MO solution treated by FST catalysts with various coating steps under UV light.

the FST2 particles was slightly higher than that of P25 under UV light irradiation, as illustrated by the curves in Figure 6. The decolorization of the MO solution of P25 started to decrease after 18 h, whereas the activity of the FST2 particles gradually increased. This finding further suggests that the catalytic persistence of FST2 particles was better than that of P25. In summary, Figure 6 illustrates the photodegradation rates of MO solution in the following order: FST2 > P25 > FST1 > FST3 > FST4 > FST5 > blank.

The variation in photocatalytic activity among the different types of particles could be ascribed to the following reasons. In the photocatalytic decomposition of MO solution under UV irradiation, photocatalytic degradation by activated TiO_2 and photosensitization process of MO are the two causes of MO solution degradation [24, 25]. Despite the existence of the photosensitization process, titanium dioxide, not the MO molecule, primarily absorbs the photon to generate electrons and holes in the conduction and valence bands, respectively. The photogenerated holes can react with H_2O or adsorbed hydroxyl to form hydroxy radicals, which can effectively oxidize the MO molecule. Moreover, the photogenerated electron can react with the adsorbed oxygen to produce a superoxide radical anion, which can also oxidize the MO molecule to a great extent. Thus, the adsorption of MO molecules by the photocatalyst is a key reason for degradation, and the adsorption condition is dependent on the size of the specific surface area of the photocatalyst [26]. Meanwhile, titania is a key factor in the degradation of MO solution, which further explains why FST2 exhibited high photocatalytic activity based on the results of XRD (see Figure 3(a)) and TEM (see Figure 1(a)).

3.3. FST2 Recycling Capacity. We further examined the cyclic utilization rate in the photocatalytic activity of FST2 to verify the recycle activity. The photocatalytic degradation of MO solution, which is a function of irradiation time in the presence of different recycling samples, was observed to follow the first-order kinetic reaction as follows:

$$\ln\left(\frac{A_0}{A}\right) = k_{app}t, \quad (1)$$

where k_{app} is the apparent rate constant and can be selected as the basic kinetic parameter for different photocatalysts, A_0 is the initial absorbance of the MO solution, and A is the solution-phase absorbance of MO solution. Using (1), we can determine the apparent rate constant from the gradient of the graph of $\ln(A_0/A)$ against the irradiation time. Notably, k_{app} can be selected as the basic kinetic parameter for different photocatalysts, which can aid in determining the photocatalytic activity despite the previous adsorption period in the dark and MO concentration remaining in the solution. Table 2 provides the degradation kinetic parameters and apparent rate constant of FST2 with different cycles of MO degradation. These results further confirm the stable property of the generated FST2. Figure 7 illustrates that FST2 exhibited the highest value of k_{app}, that is, the highest photocatalytic capability, in the first cycle. The reduction in k_{app} after the first cycle may be attributed to the intermediates adsorbed on the surface of FST2 (carbonization) during the recycling process [27].

Table 2: Photocatalytic capability of FST2 with different cycles of MO degradation.

Cycle number	Equation	k_{app} (min^{-1})	R^2
1	$y = 4 \times 10^{-3}x$	4×10^{-3}	0.9933
2	$y = 3.5 \times 10^{-3}x$	3.5×10^{-3}	0.9962
3	$y = 3.25 \times 10^{-3}x$	3.25×10^{-3}	0.9966
4	$y = 2.75 \times 10^{-3}x$	2.75×10^{-3}	0.9982

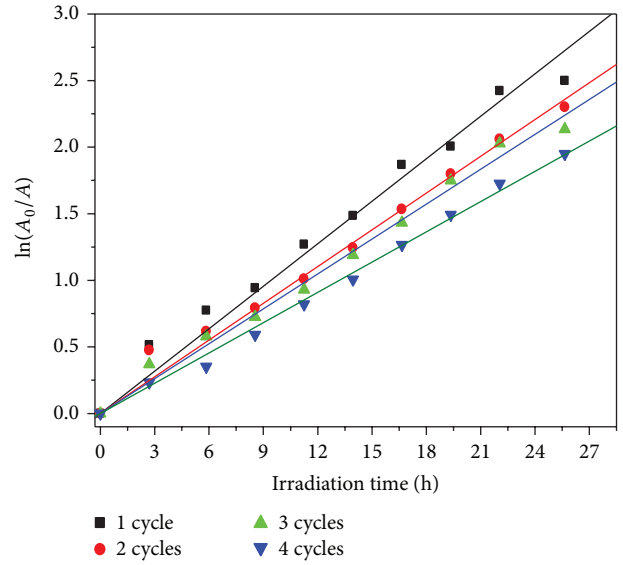

Figure 7: Plot of $\ln(A_0/A)$ versus time.

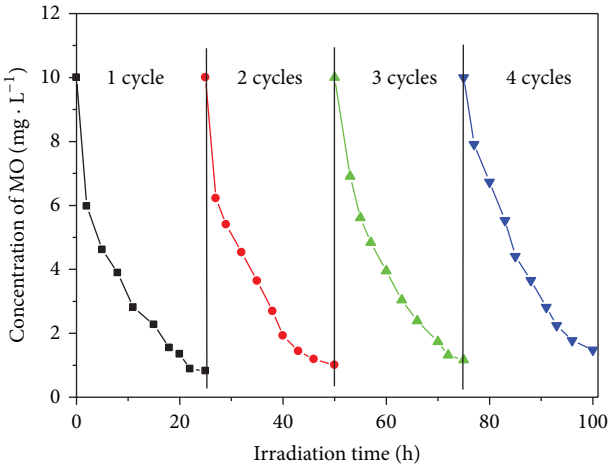

FIGURE 8: Recycling of FST2 under UV irradiation.

The photocatalytic activity of the recycled FST2 was further examined in a magnetic field, where the FST2 particles were separated. No particles were found in the degraded solution. The separated FST2 particles were used to photodegrade the MO solutions repetitively under UV irradiation, as shown in Figure 8. The photocatalytic activity of the recycled FST2 particles only changed slightly after four cycles, which indicates that the generated FST2 was stable for further applications. The experimental results also show that the separation of photocatalysts by the magnetic field was effective and the reproducibility of the photocatalytic activity of the recycled FST2 particles was satisfactory.

4. Conclusions

In this study, FST core-shell nanoparticles encapsulated for different times, represented as FST1, FST2, FST3, FST4, and FST5, were obtained using the carbon reduction and sol-gel methods. The properties of these particles were characterized by SEM, TEM, XRD, and BET. The characterization results indicate that FST2 exhibited the best property in terms of photocatalytic activity among all types of particles. The results of MO decoloration showed that FST2 possessed the most significant photocatalytic effect in breaking down 10 mg/L MO by 85% under UV light over 25 h, whereas the other types of particles could not degrade the MO solution. Experiments for verifying the recycle activity were further performed, thereby indicating that the generated FST2 exhibited the highest photocatalytic activity in the first cycle and stable property in the remaining cycles. The results of these characterizations demonstrate that the recoverable FST2 exhibited good photocatalytic activity while maintaining stability for further applications.

Conflict of Interests

The authors declare that there is no conflict of interests regarding the publication of this paper.

Acknowledgments

This research was supported by the Merit-Funded Science and Technology Project for Returned Overseas Scholars from the Ministry of Human and Social Security of Shanxi Province, Natural Science Foundation (no. 2011011013-2), and Youth Foundation (no. 2011021020-2 and no. 2012021008-3) of Science and Technology Agency of Shanxi Province, China.

References

[1] H. M. Torres Galvis, J. H. Bitter, C. B. Khare, M. Ruitenbeek, A. I. Dugulan, and K. P. De Jong, "Supported iron nanoparticles as catalysts for sustainable production of lower olefins," *Science*, vol. 335, no. 6070, pp. 835–838, 2012.

[2] M. A. Kiser, P. Westerhoff, T. Benn, Y. Wang, J. Pérez-Rivera, and K. Hristovski, "Titanium nanomaterial removal and release from wastewater treatment plants," *Environmental Science and Technology*, vol. 43, no. 17, pp. 6757–6763, 2009.

[3] S. Bagheri, K. Shameli, and S. B. A. Hamid, "Synthesis and characterization of anatase titanium dioxide nanoparticles using egg white solution via sol-gel Method," *Journal of Chemistry*, vol. 2013, Article ID 848205, 5 pages, 2013.

[4] Q. Zhang, C. Xue, Y. Yuan, J. Lee, D. Sun, and J. Xiong, "Fiber surface modification technology for Fiber-Optic localized surface plasmon resonance biosensors," *Sensors*, vol. 12, no. 3, pp. 2729–2741, 2012.

[5] M. Sökmen, D. W. Allen, F. Akkaş, N. Kartal, and F. Acar, "Photo-degradation of some dyes using Ag-loaded titanium-dioxide," *Water, Air, and Soil Pollution*, vol. 132, no. 1-2, pp. 153–163, 2001.

[6] Y. Badr and M. A. Mahmoud, "Photocatalytic degradation of methyl orange by gold silver nano-core/silica nano-shell," *Journal of Physics and Chemistry of Solids*, vol. 68, no. 3, pp. 413–419, 2007.

[7] Y. M. Slokar and A. Majcen Le Marechal, "Methods of decoloration of textile wastewaters," *Dyes and Pigments*, vol. 37, no. 4, pp. 335–356, 1998.

[8] J. Li, C. Xue, Q. Zhang et al., "Investigation of TiO_2-SiO_2-Fe_3O_4 core-shell nanoparticle properties with different functional layer thickness," in *Proceedings of the IEEE International Conference on Nanotechnology*, pp. 876–879, Beijing, China, August 2013.

[9] S. S. Srinivasan, J. Wade, and E. K. Stefanakos, "Synthesis and characterization of photocatalytic TiO_2-$ZnFe_2O_4$ nanoparticles," *Journal of Nanomaterials*, vol. 2006, Article ID 45712, 4 pages, 2006.

[10] A. E. H. Machado, M. D. França, V. Velani et al., "Characterization and evaluation of the efficiency of TiO_2/zinc phthalocyanine nanocomposites as photocatalysts for wastewater treatment using solar irradiation," *International Journal of Photoenergy*, vol. 2008, Article ID 482373, 12 pages, 2008.

[11] G. Liu, J. Pan, L. Yin et al., "Heteroatom-modulated switching of photocatalytic hydrogen and oxygen evolution preferences of anatase TiO_2 microspheres," *Advanced Functional Materials*, vol. 22, pp. 3233–3238, 2012.

[12] K. E. O'Shea, E. Pernas, and J. Saiers, "Influence of mineralization products on the coagulation of TiO_2 photocatalyst," *Langmuir*, vol. 15, no. 6, pp. 2071–2076, 1999.

[13] Q. Zhang, J. Li, X. Chou, L. Gao, Z. Hai, and C. Xue, "Synthesis of superparamagnetic iron oxide nanoparticles in carbon reduction method," *Micro and Nano Letters*, vol. 8, pp. 598–601, 2013.

[14] Y. Li, H. Zhang, Z. Guo et al., "Highly efficient visible-light-induced photocatalytic activity of nanostructured AgI/TiO_2 photocatalyst," *Langmuir*, vol. 24, no. 15, pp. 8351–8357, 2008.

[15] B. Xin, Z. Ren, P. Wang, J. Liu, L. Jing, and H. Fu, "Study on the mechanisms of photoinduced carriers separation and recombination for Fe^{3+}-TiO_2 photocatalysts," *Applied Surface Science*, vol. 253, no. 9, pp. 4390–4395, 2007.

[16] W. Fu, H. Yang, M. Li et al., "Preparation and photocatalytic characteristics of core-shell structure $TiO_2/BaFe_{12}O_{12}$ nanoparticles," *Materials Letters*, vol. 60, no. 21-22, pp. 2723–2727, 2006.

[17] M. S. Lee, G.-D. Lee, S. S. Park, C.-S. Ju, K. T. Lim, and S.-S. Hong, "Synthesis of TiO_2/SiO_2 nanoparticles in a water-in-carbon-dioxide microemulsion and their photocatalytic activity," *Research on Chemical Intermediates*, vol. 31, no. 4–6, pp. 379–389, 2005.

[18] S. Watson, D. Beydoun, and R. Amal, "Synthesis of a novel magnetic photocatalyst by direct deposition of nanosized TiO_2 crystals onto a magnetic core," *Journal of Photochemistry and Photobiology A*, vol. 148, no. 1–3, pp. 303–313, 2002.

[19] H. Liu, Z. Jia, S. Ji, Y. Zheng, M. Li, and H. Yang, "Synthesis of $TiO_2/SiO_2@Fe_3O_4$ magnetic microspheres and their properties of photocatalytic degradation dyestuff," *Catalysis Today*, vol. 175, no. 1, pp. 293–298, 2011.

[20] T.-L. Su, C.-S. Chiou, and H.-W. Chen, "Preparation, photocatalytic activity, and recovery of magnetic photocatalyst for decomposition of benzoic acid," *International Journal of Photoenergy*, vol. 2012, Article ID 909678, 8 pages, 2012.

[21] T. Kojima, T. A. Gad-Allah, S. Kato, and S. Satokawa, "Photocatalytic activity of magnetically separable $TiO_2/SiO_2/Fe_3O_4$ composite for dye degradation," *Journal of Chemical Engineering of Japan*, vol. 44, no. 9, pp. 662–667, 2011.

[22] J.-W. Lee, S. Kong, W.-S. Kim, and J. Kim, "Preparation and characterization of SiO_2/TiO_2core-shell particles with controlled shell thickness," *Materials Chemistry and Physics*, vol. 106, no. 1, pp. 39–44, 2007.

[23] J. W. Lee, M. R. Othman, Y. Eom, T. G. Lee, W. S. Kim, and J. Kim, "The effects of sonification and TiO_2 deposition on the micro-characteristics of the thermally treated SiO_2/TiO_2 spherical core-shell particles for photo-catalysis of methyl orange," *Microporous and Mesoporous Materials*, vol. 116, no. 1–3, pp. 561–568, 2008.

[24] W. Z. Tang, Z. Zhang, H. An, M. O. Quintana, and D. F. Torres, "TiO_2/UV photodegradation of azo dyes in aqueous solutions," *Environmental Technology*, vol. 18, no. 1, pp. 1–12, 1997.

[25] P. Dong, B. Liu, Y. Wang, H. Pei, and S. Yin, "Enhanced photocatalytic activity of (Mo, C)-codoped anatase TiO_2 nanoparticles for degradation of methyl orange under simulated solar irradiation," *Journal of Materials Research*, vol. 25, no. 12, pp. 2392–2400, 2010.

[26] D. S. Kim, S. J. Han, and S.-Y. Kwak, "Synthesis and photocatalytic activity of mesoporous TiO_2 with the surface area, crystallite size, and pore size," *Journal of Colloid and Interface Science*, vol. 316, no. 1, pp. 85–91, 2007.

[27] M. Long, W. Cai, J. Cai, B. Zhou, X. Chai, and Y. Wu, "Efficient photocatalytic degradation of phenol over $Co_3O_4/BiVO_4$ composite under visible light irradiation," *Journal of Physical Chemistry B*, vol. 110, no. 41, pp. 20211–20216, 2006.